Periodico di Mineralogia (2012), 81, 1, 35-59 DOI: 10.2451/2012PM0003

**PERIODICO di MINERALOGIA**
*established in 1930*

***An International Journal of***
*MINERALOGY, CRYSTALLOGRAPHY, GEOCHEMISTRY,*
*ORE DEPOSITS, PETROLOGY, VOLCANOLOGY*
and applied topics on *Environment*, *Archeometry* and *Cultural Heritage*

# Spinel-peridotites of the Frido Unit ophiolites (Southern Apennine-Italy): evidence for oceanic evolution

Maria T. Cristi Sansone[1,*], Giacomo Prosser[2], Giovanna Rizzo[3] and Paola Tartarotti[4]

[1]Dipartimento di Strutture, Geotecnica, Geologia Applicata (DiSGG) -
Università degli Studi della Basilicata, 85100 Potenza, Italy
[2]Dipartimento di Scienze Geologiche - Università degli Studi della Basilicata, 85100 Potenza, Italy
[3]Dipartimento di Chimica - Università degli Studi della Basilicata, 85100 Potenza, Italy
[4]Dipartimento di Scienze della Terra - Università degli Studi di Milano, Italy
*Corresponding author: *mariacristisansone@virgilio.it*

## Abstract

The ophiolitic rocks of the Frido Unit include serpentinites derived from a lherzolitic and subordinately harzburgitic mantle, as suggested by microstructural and petrographical features. The serpentinites are englobed in tectonic slices where they are associated with metadolerite dykes and medium to high-grade metamorphic rocks such as amphibolite, gneiss, granofels as well as gabbro and basalt with pillow structures. The matrix of tectonic slices is mainly composed of calcschists and phyllites. The serpentinites of the Frido Unit show pseudomorphic and vein textures. Primary mantle minerals are represented by olivine, clinopyroxene, orthopyroxene and orthopyroxene exolutions, and spinel and are identifiable by of the occurrence of either fresh minerals or pseudomorphs maintaining the mineral shape. Pseudomorphic minerals are serpentine, magnetite, chlorite, and amphibole. Olivine is replaced by serpentine forming a mesh texture; orthopyroxene is mostly altered to bastite; in some cases it shows exsolution lamellae of clinopyroxene and kink bands; fresh orthopyroxene is preserved as exsolution inside clinopyroxene porphyroclasts. Clinopyroxene is armoured by amphibole rim. Spinel shows a holly-leaf habit and is often armoured by a corona of Cr-chlorite. The core of the analyzed spinel has a Cr-Al spinel composition corresponding to chromite ($Al_2O_3$=29-31 wt%; $Cr_2O_3$= 28-37 wt%), whereas the rim has a Fe-Cr spinel composition corresponding to ferritchromite ($Al_2O_3$= 1-2% wt; $Cr_2O_3$=28-30 wt%). The Cr-Al spinel/ferritchromite ratio may be various in different spinel porphyroclasts. Magnetite replaces spinel or occurs within the mesh textured serpentine. The metamorphic assemblages in the Frido Unit serpentinites allow to infer qualitatively the physical conditions operating during serpentinization. The metamorphic mineral assemblages are typical of the greenschist-amphibolite transition and greenschist facies conditions, as suggested by the occurrence of tremolite/actinolite replacing clinopyroxene and of Cr-chlorite and ferritchromite after Al-

rich chromite. These minerals were produced by interactions between hydrothermal fluids and mantle peridotites. Serpentinites are cut by veins filled with mineralogical assemblages typical of the prehnite-pumpellyite facies, likely related to later orogenic Apennine evolution, as observed in the surrounding rocks of the same tectonic unit. Instead, early orogenic LT blueschist facies minerals recorded in the nearby metadolerite dykes were not observed in the serpentinites.

*Key words*: Southern Apennine; Frido Unit; ocean-floor metamorphism; ophiolites; serpentinites; spinel.

## Introduction

The serpentinites of the Frido Unit (Liguride Complex, Southern Apennines) were studied in order to define their nature (i.e., mantle vs. crust origin) and their metamorphic evolution. These serpentinites are englobed in tectonic slices where they are associated with mafic dykes and medium to high-grade metamorphic rocks such as amphibolite, gneiss, granofel as well as gabbro and basalt with pillow structures. The matrix of tectonic slices is mainly composed of calchschists and phyllites. The Frido Unit serpentinites were collected at San Severino Lucano village and at Fosso Arcangelo, located at the Calabria-Lucanian border (Figures 1, 2).

Serpentinization process occurs through hydration of peridotites by the introduction of seawater in the oceanic lithosphere, made possible by the presence of fractures and large faults driving seawater at depth (e.g., Aumento and Loubat, 1971; Prichard, 1979; Escartin et al., 1997). The extent of serpentinization depends on several parameters, as rock permeability and porosity, but also on the structural level of the mantle rocks in the lithosphere. Serpentinization is more pervasive in mantle rocks near the seafloor, as it presently occurs in the Atlantic Ocean (e.g. Boillot et al., 1988; 1989; Karson et al., 1987; Kelemen et al., 2004). Serpentinization is responsible for a strong decrease in rock density infact, fresh peridotite has a density of 3.3 gr/cm$^3$ and serpentinite has a density of 2.5 gr/cm$^3$. Such density variation should be accompanied by either a volume change and/or a loss of chemical elements. Although an increase in volume seems to be attested by the serpentinite textures (e.g., network of extensional serpentine veins), the problem of volume increase has not completely unravelled (Mével, 2003).

The geodynamic setting of the Frido Unit ophiolites can be referred to the Jurassic Tethyan ocean, and serpentinites could represent the mantle portions exposed on the Tethyan seafloor, similarly to what is presently observed in the Atlantic or Indian oceans, where extensive serpentinization has been documented by several sampling surveys (Aumento e Loubat, 1971; Bonatti, 1968; Bonatti, 1976; Cannat et al., 1997; Mével et al., 1991; Miyashiro et al., 1969). The western Tethys has been interpreted by several Authors as comparable to the modern slow-spreading oceans, as the Atlantic (Lemoine et al., 1987; Lagabrielle and Cannat, 1990; Lagabrielle and Lemoine, 1997; Cannat, 1996; Cannat et al., 1997, Magde et al., 2000; Rabain et al., 2001). This inference can be also supported by the occurrence, in the Frido Unit ophiolites, of doleritic dykes intruded in the serpentinites (Sansone et al., 2011; Sansone, 2009). Infact this evenience seems to be a peculiar character of the alpine western Tethys ophiolites and it is comparable to what is seen in the modern oceanic crustal sections exposed along the Mid-Atlantic Ridge (Lagabrielle and Lemoine, 1997). Evidence of mantle exposure in the alpine Tethyan ophiolites have been documented by several authors from the Alps, Apennines, and

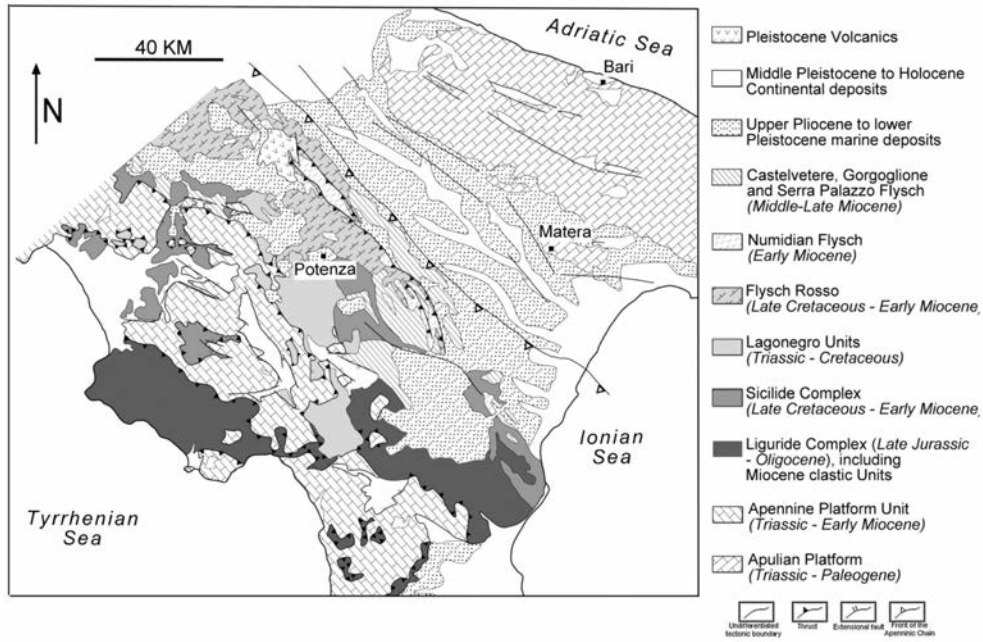


Figure 1. Sketch map of Southern Apennine (Modified after Piedilato and Prosser, 2005).

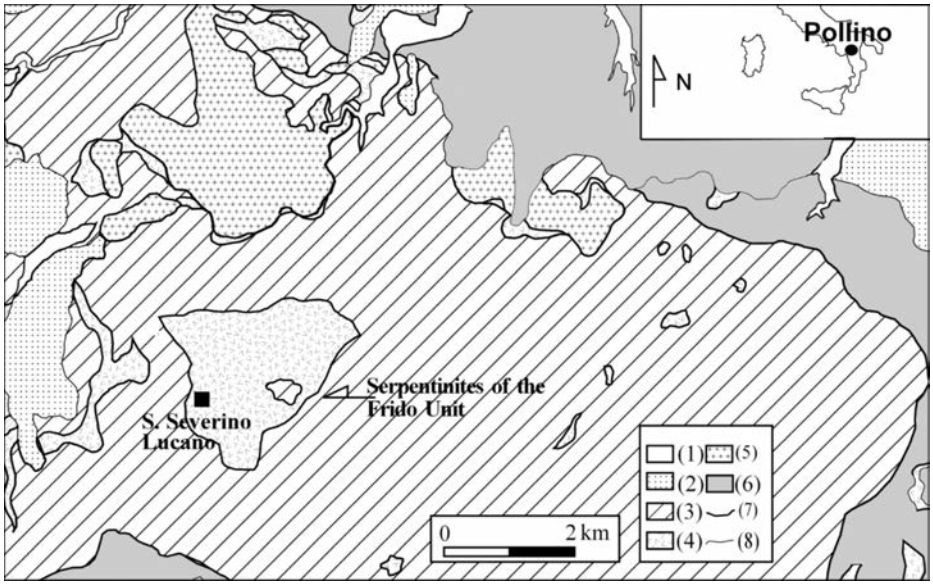


Figure 2. Geological map of the Liguride Unit crop out near Pollino Ridge (Sansone et al., 2011, modified after Monaco et al., 1995). (1) Alluvial deposits; (2) Pleistocene deposits; (3) Frido Unit; (4) Ophiolites; (5) Amphibolites, gneiss, and granofels; (6) North-Calabrian Unit; (7) Faults; and (8) Stratigraphic limit.

Corse (Cortesogno et al., 1994; Driesner, 1993; Lagabrielle et al., 1984; Tartarotti et al., 1998; Treves and Harper, 1994). We focused our study on the textures and mineral chemistry of selected samples of the Frido Unit serpentinites, in order to characterize the nature of their protolith and their metamorphic evolution, with the main purpose of deciphering the oceanic to orogenic history.

## Geological setting of the Southern apennines ophiolites

The Southern Apennines (Figure 1) are a fold-and-thrust belt formed between the Upper Oligocene and the Quaternary during the convergence between the African and European plates with closure of the Tethyan ocean and the simultaneous retreat to southeast of the Ionian subduction (Gueguen et al., 1998; Cello and Mazzoli, 1999; Doglioni et al., 1999; Patacca and Scandone, 2007). In the Southern Apennines, ophiolites are extensively exposed in the northeastern slope of the Pollino Ridge (Figure 2). Ophiolites are part of the Liguride Complex (Ogniben, 1969) and have been attributed by many Authors to the Jurassic Tethyan ocean (Vezzani, 1970; Amodio-Morelli et al., 1976; Spadea, 1976; 1982; 1994; Knott, 1987; 1994; Lanzafame et al., 1979; Tortorici et al., 2009) which began to open, together with the Atlantic Ocean, in the Middle Jurassic and closed during the Late Cretaceous-Eocene.

The Liguride Complex consists of tectonic units including sedimentary and metamorphic sequences of Upper Jurassic to Upper Oligocene age (Monaco and Tortorici, 1994). These units englobe several bodies of oceanic as well as continental crust (Vezzani, 1969). The tectonic units of the Liguride Complex are covered by turbidite sequences of Mid-Late Oligocene to Early-Mid Miocene (Bonardi et al., 1988; Monaco, 1993). The Liguride Complex has been interpreted by some Authors as the suture zone between the converging paleo-Europe and paleo-African plates (Ogniben, 1969; Knott, 1987; 1994; Monaco et al., 1991; Tortorici et al., 2009). According to this view, the Southern Apennine ophiolites derived from the Liguride ocean which was bordered by two main transform faults, i.e., the Pirenaic Fault to the north, and the Azor-Gibraltar Fault, to the south (Tortorici et al., 2009 and references therein). Alternatively, the Liguride Complex would pertain, at least in part (i.e., the metamorphic sequences of the Frido Unit) to the early-Alpine, European-vergent chain, subsequently englobed in the Apennine chain (Amodio-Morelli et al., 1976; Bonardi et al., 1988).

The internal setting of the Liguride Complex Auct. has been revised by Bonardi et al. (1988) who identified as Liguride Units only the lower part of the Liguride Complex defined by Ogniben (1969). According to Bonardi et al. (1988), the Liguride Units consist, from top to bottom, of the Frido Unit, the Episcopia-San Severino Mélange, the Northern Calabrian Unit, and the Sicilian-type terranes. The former three units have an oceanic origin, whilst the fourth has a continental nature (Bonardi et al., 2009). The Frido Unit and the Episcopia-San Severino Mélange show an orogenic HP-LT metamorphic imprint (Spadea, 1994; Sansone et al., 2011); the Northern Calabrian Unit has been affected only by oceanic alteration (Lanzafame et al., 1978) and is avoid of any orogenic metamorphism. The Sicilian-type terranes consist of rocks similar to those found in the North Calabrian Sicilian Units (i.e., “Argille Varicolori”; Bonardi et al., 2009). More recently, the Liguride Units have been divided into three main tectonic units (Monaco and Tortorici, 1994): i) the Calabro-Lucano Flysh (Monaco et al., 1991), a unmetamorphosed unit which partly corresponds to the North-Calabrian Unit defined by Bonardi et al. (1988); ii) the metamorphic terranes of the Frido Unit (Vezzani, 1969; Amodio-Morelli et al., 1976); iii) syn-orogenic turbiditic sequences, i.e., the

Saraceno Formation, the Albidona Formation, and a sequence consisting of alternating shales, mudstones, and sandstones, this latter corresponding to the Perosa unit as defined by Vezzani (1966). More recent studies (Di Leo et al., 2005; Laurita et al., 2009) basically support the model proposed by Monaco and Tortorici (1994), by confirming the structural location of the Frido Unit at the top of the Liguride Units.

The ophiolites of the Southern Apennine Liguride Units occur in the Frido Unit and in the North-Calabrian Unit (Figure 2). The ophiolitic rocks of the Frido Unit consist of serpentinites and minor metagabbros, metabasalt, diabase (some with relict pillow structures), and their respective sedimentary cover (Vezzani, 1970; Spadea, 1982; 1994). This Unit is characterized by blueschist-facies metamorphic imprint. The Frido Unit also includes high-to-medium grade metamorphic rocks of continental origin (gneiss, granofels, and amphibolites). The ophiolites of the North Calabrian Unit (Timpa delle Murge-Timpa Pietrasasso sequences) are made of pillow lavas and pillow breccias, hyaloclastites, diabase, and scarce Mg-gabbro cumulates covered by siliceous shales, radiolarian cherts, and limestones (Lanzafame et al., 1979). In these ophiolites the orogenic metamorphic imprint is weak or absent (Lanzafame et al., 1978).

## The Frido Unit

The Frido Unit (Amodio-Morelli et al., 1976) almost entirely corresponds to the Frido Formation defined by Vezzani (1969). This unit is exposed for about 10 km, from the Frido Valley to NW, to the Sarmento valley, to SE. It is overthrust on the North-Calabrian Unit (Di Leo et al., 2005) as well as on the Calabro-Lucano Flysch (Monaco and Tortorici, 1994). Overall, the Frido Unit is composed of metamorphic rocks englobing olistoliths of various size made of ophiolite and basement rocks of continental origin. Monaco and Tortorici (1994) have divided this Unit into a lower sub-unit mainly consisting of shales, and an upper unit made of calcschists; the two sub-units are separated by serpentinites. They are mostly made of cataclastic serpentinites, metabasalts, and rodingite. Serpentinites are associated with garnet-bearing gneiss, granofels, and amphibolite (Spadea, 1982 and references therein), showing mineral assemblages of the the lawsonite-facies and of the pumpellyite + aragonite facies metamorphism, although crossite, Mg-riebeckite, and aegirine-augite have been observed (Spadea, 1982). These blocks of the Frido Unit have been interpreted as a tectonic mélange (Bonardi et al., 1988; Knott, 1987).

The metamorphic imprint of the Frido Unit rocks is characterized by HP-LT conditions under the blueschist facies (Spadea, 1994) and has been interpreted by some Authors as related to an early orogenic event followed by a later retrogression under the greenschist facies (Cello and Mazzoli, 1999). However, this interpretation is not supported by the occurrence of glaucophane rimming tremolite in metadolerite dykes (Sansone, 2006; Sansone et al., 2011). This occurrence provides an evidence for an orogenic blueschist facies metamorphism following an oceanic alteration stage under greenschist facies conditions (Laurita, 2008; Sansone et al., 2011). The physical conditions of the orogenic metamorphism have been estimated in the ophiolites of the Frido Unit at P = 6-8 kbar and T = 200-300 °C (Spadea, 1994; Sansone et al., 2011). Similar conditions have been obtained by fluid inclusions studies in some metasediments (Invernizzi et al., 2008), whereas thermobaric conditions of 11-13 kbar and 280-320 °C have been estimated by Cavalcante et al. (2009) in the metapelites from the southern Frido Unit. Metamorphic and structural features of the Frido Unit have been referred to an accretionary wedge setting (Knott, 1987; 1994; Monaco et al., 1991; Monaco and Tortorici, 1995). Namely, Knott (1987; 1994) has interpreted the Frido Unit as

being part of an accretionary wedge formed during the NW-oriented subduction of the Liguride sector of the Tethyan ocean starting in the Late Cretaceous.

## Petrographic features of the Frido Unit serpentinites

Eight samples of serpentinite from the Frido Unit (FU) were collected near San Severino Lucano: the serpentinites studied are distinguished by into in cataclastic and massive. Modal composition of the serpentinized perodotites may be reconstructed with the following assumptions (Juteau et al., 1990): the mesh texrure and magnetite in the serpentine matrix are counted as olivine, bastite pseudomorphs are assigned to primary orthopyroxene, magnetite rimming the Cr-spinel is counted as primary spinel. Based on the above assumptions these rocks may be classified as lherzolite and harzburgite (Table 1).

Serpentinites of FU are characterized by two main different textures: pseudomorphic and vein textures. Pseudomorphic texture is represented by mesh texture (Wicks and Whitaker, 1977; Wicks et al., 1977; Prichard, 1979) defined by serpentine + magnetite that statically replace the olivine crystals (Figure 3a, b), and by yellow-brown bastite replacing orthopyroxene. Vein texture is represented by various submillimetric veins which cut each other and crosscut the pseudomorphic texture.

In spite of their extensive serpentinization, the FU serpentinites still preserve relict fresh minerals such as olivine, spinel, and various amounts of clinopyroxene pertaining to the original peridotite mineral assemblage. Orthopyroxene was observed as fresh porphyroclasts as well as bastite pseudomorphs that still preserve the orthopyroxene prismatic habit; fresh orthopyroxene also occurs as exsolution lamellae within clinopyroxene porphyroclasts. Secondary minerals are serpentine, chlorite, magnetite, prehnite, and amphibole; accessory minerals are epidote and Fe-hydroxides.

Fresh olivine is locally still recognizable at the core of serpentine + magnetite pseudomorphs in the mesh and ribbon textures (Figure 3b), since replacement of olivine by serpentine + magnetite, according to the general reaction in a Mg-Fe-rich system "olivine + seawater = serpentine + magnetite + $H_2$" (Mével, 2003) proceeds from the external rim to the core of olivine porphyroblast (Prichard, 1979). Fine-grained magnetite commonly forms networks in the serpentinized matrix. Orthopyroxene porphyroclasts, although replaced by serpentine pseudomorphs (bastite), are still recognizable for the elongated ovoidal shape (Figure 4), the millimetric size, and occurrence of clinopyroxene exsolution lamellae. Orthopyroxene porphyroclasts are characterized by a weak shape preferred orientation defining a weak foliation. In some samples, kinked orthopyroxene is replaced by pseudomorphs of amphibole (Figure 5), interpreted as being of the tremolite-actinolte series on the basis of optical characters.

Clinopyroxene porphyroclasts are subeuhedral and are often rimmed by amphibole interpreted as being of the tremolite-actinolite series on the basis of optical characters (Figure 6). Spinel forms red-brown coloured xenomorphic, holly-leaf-shaped porphyroclasts (Figure 7). This habit has been defined as typical of porphyroclastic mantle peridotites (Mercier and Nicolas, 1975). Spinel porphyroclasts are always rimmed by fine-grained chlorite (see next chapter). In some samples spinel is replaced by pseudomorphic magnetite occurring in fine-grained crystal aggregates.

The FU Serpentinites are cut by various types of veins filled with serpentine, chlorite, amphibole, prehnite, and a brown-coloured mineral undetectable under the optic microscope. Veins filled with serpentine are commonly less than 1 mm-thick and are arranged in sets of parallel veins responsible of the apparent

Table 1. Mineralogical assemblages of the serpentinites.

| Sample | Pseudomorphic texture | Primary assemblage | Metamorphic minerals | Type | Mantle peridotites | Locality of sampling |
|---|---|---|---|---|---|---|
| SPR1 | Mesh texture | Ol (70%), Spl (10%), Cpx (10%), and fresh Opx (5%) | Srp, Op, Chl, Pmp, Ep, and Cpx exsolution lamellae | cataclastic | Lherzolite | Fosso Arcangelo |
| SPR2 | Mesh texture and bastite | Ol (60%), Spl (15%), Cpx (15%), and Opx (3%) | Srp, Op, Chl, Prh*, Ep, and Cpx exsolution lamellae | cataclastic | Lherzolite | Fosso Arcangelo |
| S1 | Mesh texture and bastite | Ol (65%), Opx (20%), Spl (10%), and relics Cpx (3%) | Srp, Op, Chl | massive | Harzburgite | S.Severino Lucano village |
| S2 | Mesh texture and bastite | Ol (65%), Opx (20%), Spl (10%), and relics Cpx (3%) | Srp, Op, Chl | massive | Harzburgite | S.Severino Lucano village |
| S3 | Mesh texture | Ol (70%), Cpx (10%), Spl (10%), and fresh Opx (5%) | Srp, Op, Chl, and Cpx exsolution lamellae | cataclastic | Lherzolite | Fosso Arcangelo |
| S4 | Mesh texture, bastite | Ol (75%), Spl (5%), Cpx (10%), and Opx (5%) | Srp, Op, Chl, and Cpx exsolution lamellae | cataclastic | Lherzolite | Fosso Arcangelo |
| S5 | Mesh texture and bastite | Ol (70%), Cpx (10%), Sp (10%), and fresh Opx (5%) | Srp, Op, Chl, Am, and Cpx exsolution lamellae | cataclastic | Lherzolite | Fosso Arcangelo |
| S6 | Mesh texture and bastite | fresh Ol (55%), Cpx (20%), Sp (10 %), and Opx (10%) | Srp, Op, Chl, Prh*, Am, and Cpx exsolution lamellae | cataclastic | Lherzolite | Fosso Arcangelo |

Symbols as in Siivola and Schmid (2007); the exception Prh* = prehnite.

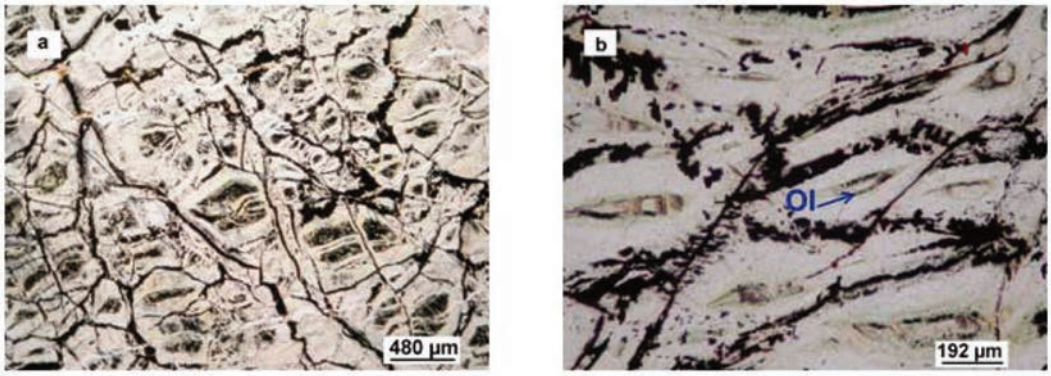


Figure 3. (a) Mesh texture; 1N, 4X. (b) Fresh olivine at the core of the mesh to ribbon texture; 1N, 10X.


Figure 4. Orthopyroxene porphyroblasts replaced by bastite and crosscut by veins of serpentine; NX, 2X.

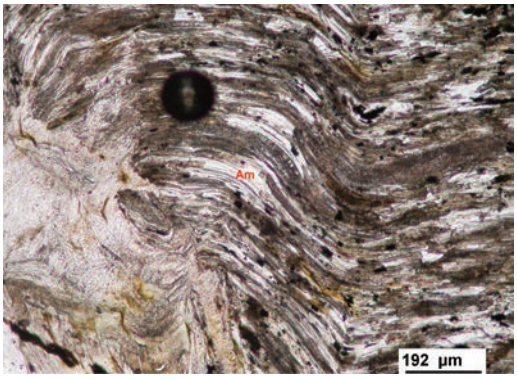


Figure 5. Orthopyroxene deformed by kink fold band; 1N, 10X.

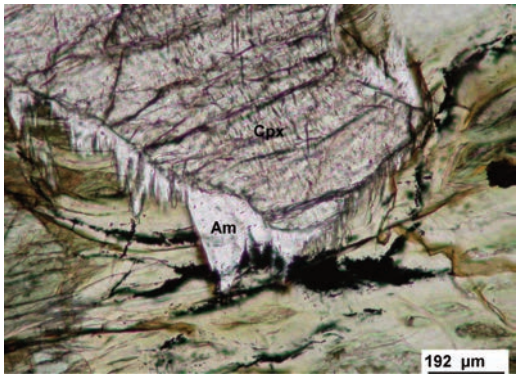


Figure 6. Clinopyroxene porphyroclasts rimmed by acicular amphibole; 1N, 10X.

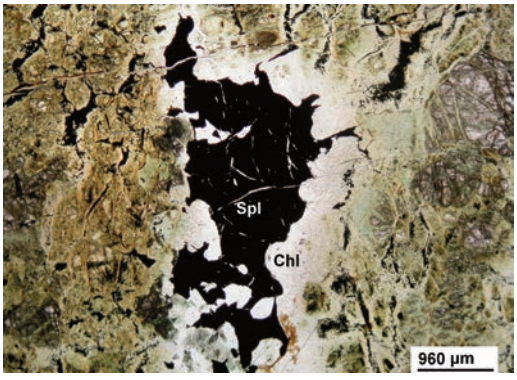


Figure 7. Spinel holly-leaf-shaped porphyroclasts; 1N, 2X.

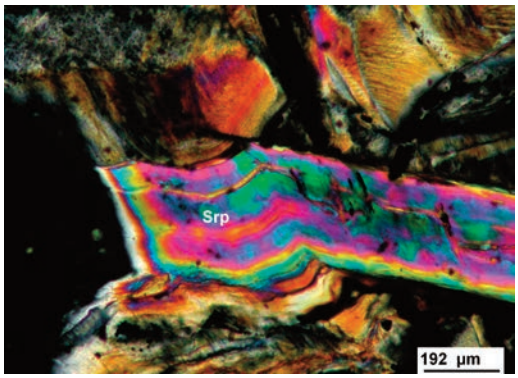


Figure 8. Vein of serpentine folded; NX, 10X.

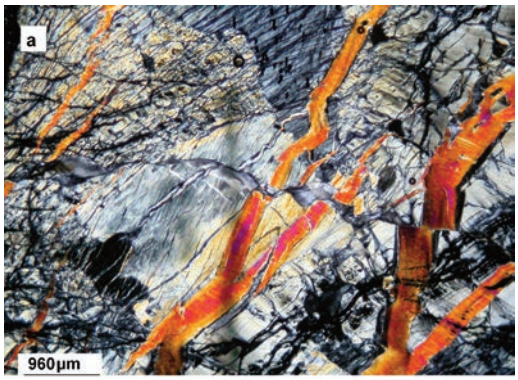


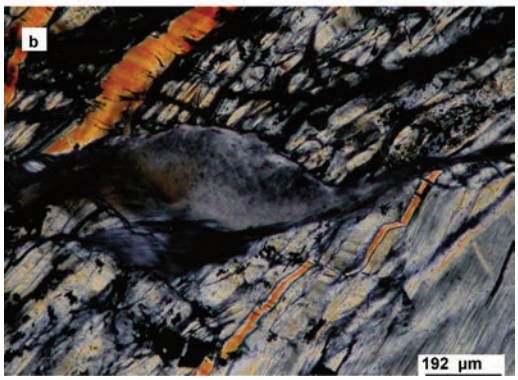


Figure 9. (a) Transtensional veins filled with serpentine; 2X, NX. (b) Micro-pull-aparts structure; 10X, NX.

foliation of the rock (Figure 4). These veins may be interpreted as extensional veins being filled with fibers orthogonal to the vein walls; veins are locally offset by microfaults or may be folded (Figure 8). Shear veins filled with serpentine fibers parallel to the vein walls were also observed. Finally, micro pull-aparts filled with serpentine fibers were observed and interpretd as being transtensional veins (Figure 9a, b).Veins filled with chlorite also occur. The latest generation veins are filled with prehnite and cut through all the previous veins and the pseudomorphic texture. Prehnite crystals commonly form fan-shaped aggregates oriented at a high angle with the vein walls (Figure 10).

On the basis of textural features shown by relict primary mineralogy, as well as by pseudomorphic serpenitinization and veining, the studied serpentinites are interpreted as original mantle abyssal spinel-peridotites bearing a porphyroclastic texture.

## Mineral chemistry

In selected samples of the FU serpentinites electron microprobe analyses were carried out on spinel, pyroxenes, serpentine, and chlorite by using a JEOL JXA-8200 probe, equipped with five WDS spectrometers and an EDS

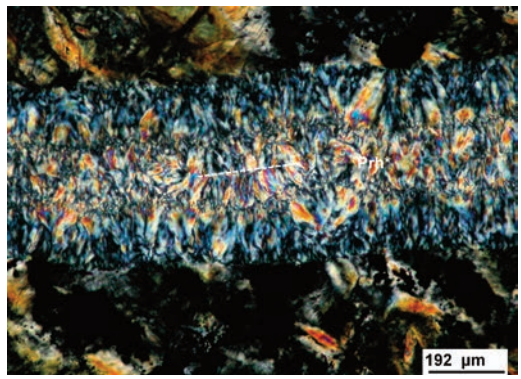


Figure 10. Prehnite vein with syntaxial texture; NX, 10X.

spectrometer, at the Dipartimento di Scienze della Terra "Ardito Desio" of the University of Milan. The analytical conditions were: 15 kV accelerating voltage and 15 nA beam current; count time 30 s at peak and 10 s at background. Natural oxides were used as standards. The symbols for minerals recommended by Siivola and Schmid (2007) were used in the text, tables, and figures; the exceptions are indicated by the following symbols: Cch* (Clinochlore); Crp* (Corundophilite); Fe-Chr* (ferritchromite); Prh* (prehnite); Shr* (Sheridanite) and Tlc-Chl* (Talc-chlorite).

*Spinel*

Structural formula of spinel was recalculated on the basis of 32 oxygens and expressed in atoms per formula unit (a.p.f.u.) as reported in Table 2. The analyzed spinel porphyroclasts are characterized by a strong chemical zonation with Al-rich cores and Fe-Cr-rich rims, as shown in the Chromite-Spinel-Magnetite diagram of Figure 11. The Cr# (100*Cr/Cr + Al) ranges between 43 and 46 in the spinel core and between 87 and 93 in the spinel rim (Table 2). The Mg content ranges between 4.862 and 5.140 a.p.f.u. at the core and between 1.203-2.251 a.p.f.u. at the rim. Manganese content is very low at the core (MnO = 0.06-0.11 wt%), whilst it is as high as 5.41 wt% at the rim (Table 2). Accordingly, the spinel core has a Al-chromite composition, whereas the spinel rim has a ferritchromite composition.

Detailed WDS/EDS compositional maps were performed on spinel porphyroclasts of sample S2 (massive serpentinite) and sample SP2R (cataclastic serpentinite) in order to show the strong compositional zonation. Compositional maps are illustrated in Figures 12, 13. The compositional maps of spinel from sample S2 clearly indicate the higher concentrations of Al at the core and of Fe and Ti at the rim (Figure 12) this latter being a ferritchromite. Chromium is homogeneously distributed (Figure 12). The compositional maps of spinel from sample SP2R (Figure 13) show that the analyzed spinel crystal is more altered than in sample S2. The composition of SP2R spinel is a ferritchromite, as evidenced by the relatively high percentage (yellow colour) of Fe which is homogenously distributed (Figure 13).

*Pyroxenes*

Structural formula of pyroxene was recalculated on the basis of 6 oxygens, the chemical composition of the analyzed pyroxenes is reported in Table 3. Clinopyroxene is characterized by homogeneous compositions rich in the diopside end-member (Morimoto, 1988; 1989), with high Al contents ($Al_2O_3$ = 4.95-6.86 wt%; Table 3) and relatively high Cr contents ($Cr_2O_3$ = 0.68-0.96 wt%; Table 3).

Chemical composition of orthopyroxene exsolutions within clinopyroxene corresponds to Enstatite (Morimoto, 1988; 1989; see analysis 173 in Table 3).

*Serpentine*

Chemical composition of serpentine is reported in Table 4, structural formula of serpentine were recalculated on the basis of 7 oxygenes. Serpentine was analyzed in the mesh texture (replacing olivine), in pseudomorph after orthopyroxene (bastite), and in the veins. Serpentine in the mesh texture and serpentine replacing orthopyroxene have in general (but not always) higher $Al_2O_3$ contents than serpentine in veins (Table 4). Serpentine replacing orthopyroxene is also characterized by higher FeO content. Serpentine in the mesh texture has commonly higher MgO contents than in other textural occurrence. Overall, the analyzed serpentine is characterized by high Cr contents: in the mesh texture $Cr_2O_3$ = 0.34-2.51 wt%; in orthopyroxene pseudomorph, $Cr_2O_3$ ranges from 0.33 wt% and 0.98 wt%, and in the serpentine vein $Cr_2O_3$ = 0.01-1.37 wt%. Nichel is characterized by low contents in all the analyzed

Table 2. Representative analyses of spinel.

| Sample | S2-C1_13 | S2-C1_14 | S2-C4-26 | S2-C4_27 | S2-C7_36 | S2-C7_37 | S2-C8_42 | S2-C8_43 | S2-C8_45 | S2-C8-46 | S2-C8_47 | S2-C8_48 |
|---|---|---|---|---|---|---|---|---|---|---|---|---|
| | core | rim | core | rim | rim | core | core | rim | semi-rim | core | semi-core | rim |
| $SiO_2$ | 0.03 | 2.57 | 0.03 | 3.28 | 4.34 | 0.03 | 0.03 | 4.21 | 0.03 | 3.83 | 0.04 | 3.98 |
| $TiO_2$ | 0.12 | 0.43 | 0.11 | 0.47 | 0.46 | 0.13 | 0.13 | 0.51 | 0.14 | 0.45 | 0.14 | 0.42 |
| $Al_2O_3$ | 30.53 | 1.56 | 29.68 | 2.24 | 3.04 | 30.40 | 31.39 | 1.85 | 30.89 | 1.90 | 30.07 | 1.61 |
| $Cr_2O_3$ | 36.39 | 28.98 | 37.27 | 32.30 | 29.86 | 35.96 | 35.52 | 30.77 | 36.03 | 29.11 | 35.44 | 29.43 |
| $Fe_2O_3$ | 4.36 | 31.93 | 4.65 | 26.61 | 26.89 | 4.70 | 4.24 | 27.80 | 4.37 | 27.77 | 5.03 | 28.60 |
| FeO | 15.59 | 25.77 | 14.47 | 25.25 | 24.66 | 15.69 | 15.81 | 24.89 | 15.94 | 24.23 | 15.06 | 24.92 |
| MnO | 0.08 | 5.13 | 0.10 | 5.41 | 4.88 | 0.11 | 0.06 | 5.33 | 0.11 | 4.91 | 0.09 | 5.03 |
| MgO | 14.06 | 2.75 | 14.69 | 3.59 | 5.35 | 13.96 | 14.08 | 4.76 | 13.95 | 4.24 | 14.20 | 4.38 |
| CaO | n.d. | 0.05 | n.d. | 0.06 | 0.09 | 0.02 | 0.01 | 0.07 | 0.01 | 0.28 | n.d. | 0.06 |
| $Na_2O$ | 0.01 | 0.02 | n.d. | 0.04 | 0.05 | n.d. | n.d. | 0.07 | 0.01 | 0.06 | n.d. | 0.04 |
| NiO | 0.14 | 0.02 | 0.12 | 0.06 | 0.02 | 0.14 | 0.13 | 0.07 | 0.10 | 0.08 | 0.10 | 0.02 |
| Sum | 101.32 | 99.22 | 101.13 | 99.31 | 99.63 | 101.14 | 101.40 | 100.34 | 101.59 | 96.86 | 100.17 | 98.51 |
| | | | | | | | | | | | | |
| Si | 0.007 | 0.754 | 0.007 | 0.948 | 1.225 | 0.007 | 0.007 | 1.193 | 0.007 | 1.127 | 0.011 | 1.154 |
| Al | 8.436 | 0.541 | 8.210 | 0.763 | 1.011 | 8.424 | 8.638 | 0.619 | 8.512 | 0.659 | 8.395 | 0.550 |
| $Fe^{3+}$ | 0.769 | 7.051 | 0.822 | 5.784 | 5.710 | 0.832 | 0.745 | 5.926 | 0.770 | 6.150 | 0.896 | 6.240 |
| $Fe^{2+}$ | 3.056 | 6.324 | 2.841 | 6.100 | 5.818 | 3.084 | 3.087 | 5.897 | 3.117 | 5.965 | 2.982 | 6.042 |
| Mg | 4.914 | 1.203 | 5.140 | 1.546 | 2.251 | 4.893 | 4.901 | 2.010 | 4.862 | 1.860 | 5.015 | 1.893 |
| Ca | 0.001 | 0.015 | 0.001 | 0.017 | 0.026 | 0.004 | 0.003 | 0.021 | 0.003 | 0.087 | 0.001 | 0.020 |
| Na | 0.006 | 0.014 | 0.001 | 0.025 | 0.028 | n.d. | 0.002 | 0.038 | 0.004 | 0.037 | 0.001 | 0.025 |
| K | 0.000 | 0.000 | 0.000 | 0.000 | 0.000 | 0.000 | 0.000 | 0.001 | 0.001 | 0.000 | 0.000 | 0.000 |
| Ti | 0.020 | 0.095 | 0.020 | 0.103 | 0.098 | 0.023 | 0.024 | 0.109 | 0.025 | 0.100 | 0.025 | 0.092 |
| Mn | 0.016 | 1.275 | 0.020 | 1.324 | 1.166 | 0.023 | 0.012 | 1.279 | 0.022 | 1.224 | 0.017 | 1.235 |
| Cr | 6.746 | 6.724 | 6.916 | 7.377 | 6.662 | 6.684 | 6.557 | 6.891 | 6.660 | 6.774 | 6.637 | 6.745 |
| Ni | 0.027 | 0.005 | 0.022 | 0.014 | 0.005 | 0.026 | 0.024 | 0.015 | 0.019 | 0.018 | 0.019 | 0.005 |
| Sum | 24.000 | 24.000 | 24.000 | 24.000 | 24.000 | 24.000 | 24.000 | 24.000 | 24.000 | 24.000 | 24.000 | 24.000 |
| Cr# | 44 | 93 | 46 | 91 | 87 | 44 | 43 | 92 | 44 | 91 | 44 | 92 |
| | Al-Chr | Fe-Chr* | Al-Chr | Fe-Chr* | Fe-Chr* | Al-Chr | Al-Chr | Fe-Chr* | Al-Chr | Fe-Chr* | Al-Chr | Fe-Chr* |

n.d. not-detected

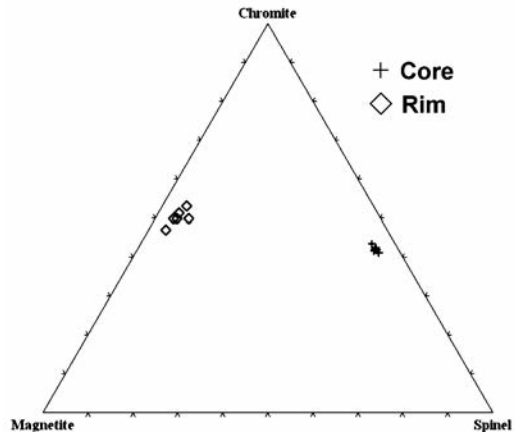


Figure 11. Spinel composition of Frido Unit: the spinel core has a Al-chromite composition, whereas the spinel rim has a ferritchromite composition.

serpentine, although in serpentine replacing olivine NiO is relatively higher (NiO = 0.24-0.39 wt%). Overall, the serpentine composition seems to inherit, at least in part, the composition of the former mineral (e.g., olivine or pyroxene).

*Chlorite*

Chlorite was recalculated on the basis of 28 oxygens as reported in Table 5 and in Figure 14 where it is classified according with Hey (1954)'s nomenclature. The analyzed chlorite occurs as rim around the spinel porphyroclasts. Chlorite in our samples is characterized by relatively high Cr contents (analyses 28, 194, 195, 198 in Table 5). In some samples, $Cr_2O_3$ is as high as 15wt% so that chlorite with $Cr_2O_3$ ranging from 3.11 wt% and 14.69 wt% can be

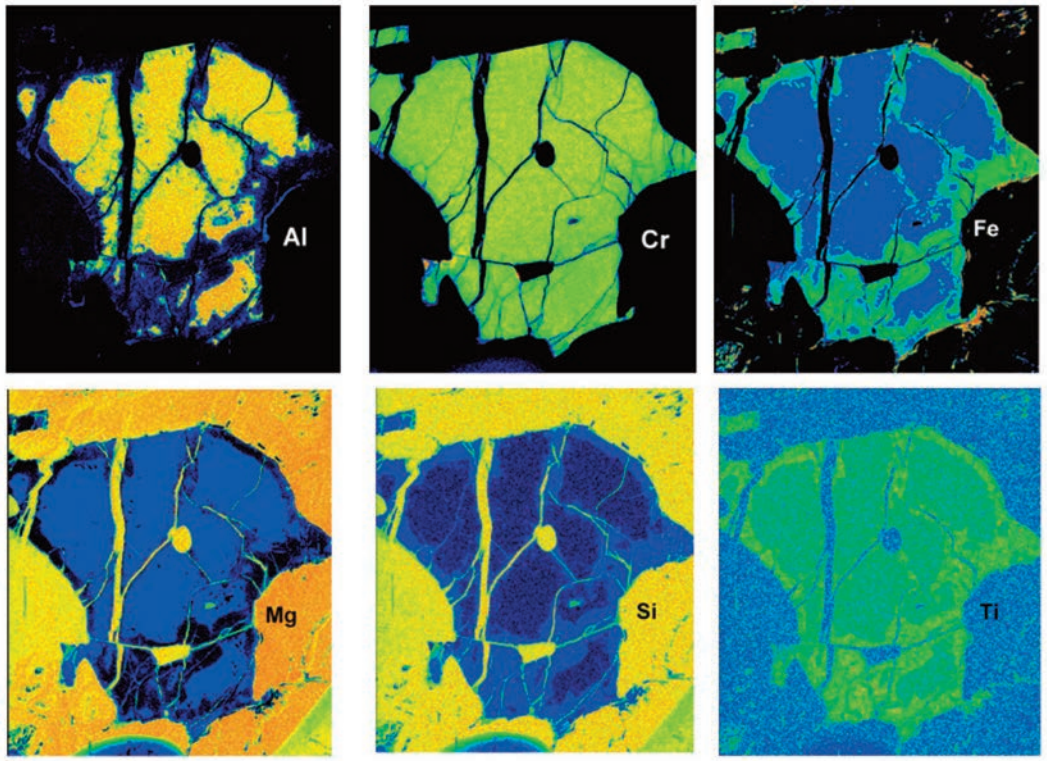


Figure 12. WDS/EDS compositional maps of major and minor element distribution in spinel porphyroclasts of sample S2 (massive serpentinite).

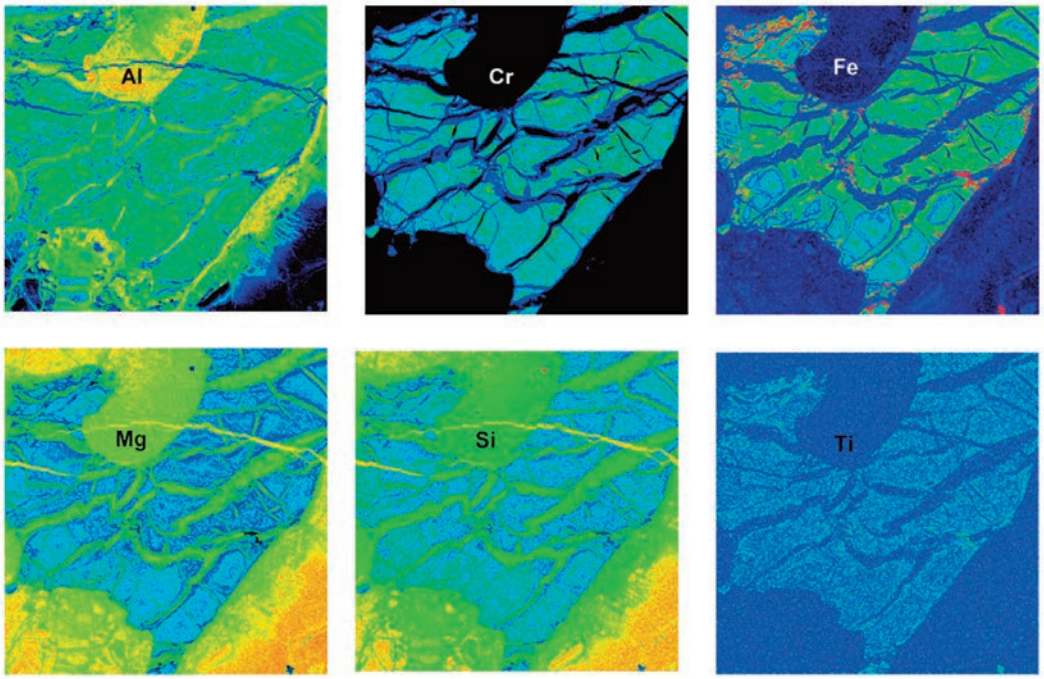


Figure 13. WDS/EDS compositional maps were of major and minor element distribution in spinel porphyroclasts of sample SPR2 (cataclastic serpentinite).

defined as Cr-chlorite, according to Swanson (2004) and to Merlini et al. (2009).

## Discussion

The ultramafic rocks of the Frido Unit are here interpreted as serpentinized mantle porphyroclastic spinel-peridotites. The foliation, that is commonly weak, is marked by the shape fabric of orthopyroxene porphyroclasts and spinel. The primary mineralogy and texture of these serpentinites can be inferred by the presence of relict primary minerals (fresh olivine, clinopyroxene, orthopyroxene and spinel) and by the pseudomorphic character of the serpentine textures. Based on these evidences and on some assumptions adopted for the modal calculations (see Table 1), the studied serpentinites can be classified as mantle lherzolite and subordinately harzburgite. Petrographic features also suggest that at least three main subsequent serpentinization events have occurred in the studied rocks: the first event corresponds to pseudomorphic replacement of olivine by serpentine, developing the typical mesh texture, and by pseudomorphic replacement of orthopyroxene by bastite. These pseudomorphs are commonly undeformed, attesting that rocks have been altered under static conditions. The second event developed veins filled with serpentine fibers growing perpendicularly to the vein wall. These veins, which may generate an apparent schistosity, record a complex history of rock fracturing, crack opening, and fluid circulation (Mével et al., 2003 and references therein). The vein network is commonly

Table 3. Representative analysis of pyroxenes.

| Sample | SP2 - C1_172 | SP2 - C1_173 | SP2 - C1_174 | SP2 - C1_175 | SP2 - C5_176 | SP2 - C5_177 | SP2 - C6_178 | SP2 - C6_179 | SP2 - C6_180 | SP2 - C6_181 | SP2 - C6_182 | SP2 - C6_183 |
|---|---|---|---|---|---|---|---|---|---|---|---|---|
| | rim | opx exsolution lamellae | rim | core | core | rim | rim | semi-core | core | core | semi-core | rim |
| $SiO_2$ | 51.21 | 54.85 | 51.31 | 51.00 | 50.65 | 51.23 | 51.91 | 51.38 | 51.12 | 51.59 | 51.27 | 52.83 |
| $TiO_2$ | 0.64 | 0.09 | 0.64 | 0.70 | 0.73 | 0.83 | 0.64 | 0.60 | 0.68 | 0.61 | 0.67 | 0.58 |
| $Al_2O_3$ | 6.43 | 4.80 | 6.15 | 6.34 | 6.86 | 6.76 | 5.60 | 6.15 | 6.49 | 6.70 | 6.56 | 4.95 |
| $Cr_2O_3$ | 0.90 | 0.56 | 0.91 | 0.89 | 0.92 | 0.90 | 0.73 | 0.82 | 0.84 | 0.92 | 0.93 | 0.68 |
| FeO | 3.18 | 8.17 | 3.08 | 3.07 | 2.96 | 2.88 | 3.07 | 3.13 | 3.23 | 3.11 | 3.04 | 3.36 |
| MnO | 0.09 | 0.17 | 0.08 | 0.08 | 0.06 | 0.06 | 0.08 | 0.07 | 0.11 | 0.10 | 0.10 | 0.05 |
| MgO | 14.54 | 31.37 | 14.83 | 14.62 | 14.42 | 14.39 | 14.93 | 14.69 | 14.39 | 14.41 | 14.49 | 16.65 |
| CaO | 22.45 | 1.07 | 22.49 | 22.53 | 22.18 | 22.47 | 22.37 | 22.14 | 22.50 | 22.15 | 22.50 | 20.79 |
| $Na_2O$ | 0.95 | 0.04 | 0.82 | 0.86 | 1.05 | 0.98 | 0.99 | 1.01 | 0.98 | 1.08 | 0.96 | 0.77 |
| $K_2O$ | n.d. | n.d. | n.d. | 0.01 | n.d. | n.d. | 0.01 | n.d. | n.d. | n.d. | n.d. | 0.01 |
| Sum | 100.39 | 101.19 | 100.33 | 100.11 | 99.88 | 100.52 | 100.33 | 100.07 | 100.40 | 100.71 | 100.54 | 100.72 |
| Si | 1.860 | 1.892 | 1.864 | 1.858 | 1.848 | 1.856 | 1.883 | 1.871 | 1.858 | 1.865 | 1.859 | 1.900 |
| $Al^{IV}$ | 0.140 | 0.108 | 0.136 | 0.142 | 0.152 | 0.144 | 0.117 | 0.129 | 0.142 | 0.135 | 0.141 | 0.100 |
| $Al^{VI}$ | 0.135 | 0.087 | 0.127 | 0.130 | 0.143 | 0.144 | 0.123 | 0.135 | 0.136 | 0.150 | 0.139 | 0.110 |
| $Fe^{3+}$ | 0.017 | 0.004 | 0.009 | 0.014 | 0.023 | n.d. | 0.012 | 0.013 | 0.020 | 0.001 | 0.010 | n.d. |
| Cr | 0.026 | 0.015 | 0.026 | 0.026 | 0.027 | 0.026 | 0.021 | 0.024 | 0.024 | 0.026 | 0.027 | 0.019 |
| Ti | 0.017 | 0.002 | 0.017 | 0.019 | 0.020 | 0.023 | 0.017 | 0.016 | 0.019 | 0.017 | 0.018 | 0.016 |
| $Fe^{2+}$ | 0.080 | 0.231 | 0.085 | 0.079 | 0.067 | 0.087 | 0.081 | 0.082 | 0.078 | 0.093 | 0.082 | 0.101 |
| Mn | 0.003 | 0.005 | 0.003 | 0.002 | 0.002 | 0.002 | 0.002 | 0.002 | 0.003 | 0.003 | 0.003 | 0.002 |
| Mg | 0.787 | 1.613 | 0.803 | 0.794 | 0.784 | 0.777 | 0.808 | 0.797 | 0.780 | 0.777 | 0.783 | 0.893 |
| Ca | 0.874 | 0.040 | 0.875 | 0.879 | 0.867 | 0.872 | 0.870 | 0.864 | 0.876 | 0.858 | 0.874 | 0.801 |
| Na | 0.067 | 0.003 | 0.058 | 0.061 | 0.074 | 0.069 | 0.070 | 0.071 | 0.069 | 0.075 | 0.067 | 0.054 |
| K | 0.000 | 0.000 | 0.000 | 0.000 | 0.000 | 0.000 | 0.000 | 0.000 | 0.000 | 0.000 | 0.000 | 0.000 |
| Sum | 4.006 | 4.001 | 4.003 | 4.005 | 4.008 | 3.999 | 4.004 | 4.004 | 4.006 | 4.000 | 4.003 | 3.996 |
| Wo | 47.810 | 2.084 | 47.769 | 48.058 | 47.705 | 48.252 | 47.199 | 47.206 | 47.963 | 47.471 | 48.023 | 43.295 |
| En | 43.089 | 85.092 | 43.833 | 43.396 | 43.159 | 43.001 | 43.836 | 43.586 | 42.687 | 42.976 | 43.037 | 48.251 |
| Fs | 5.430 | 12.683 | 5.240 | 5.233 | 5.066 | 4.924 | 5.181 | 5.325 | 5.551 | 5.378 | 5.232 | 5.556 |
| Aeg | 3.670 | 0.140 | 3.159 | 3.313 | 4.069 | 3.823 | 3.784 | 3.883 | 3.799 | 4.176 | 3.708 | 2.898 |

n.d. not-detected

Table 4. Representative analysis of serpentine.

| Sample | S2-C2_8 | S2-C2_9 | S2-C2_10 | S2-C2_11 | S2-C2_12 | S2-C1_15 | S2-C1_16 | S2-C1_17 | S2-C1 _18 | S2-C1_19 | S2-C1_20 |
|---|---|---|---|---|---|---|---|---|---|---|---|
| | pseudomorph after Px | pseudomorph after Px | pseudomorph after Px | bastite | bastite | pseudomorph after Spl | mesh texture | mesh texture | mesh texture | core of mesh texture | rim of mesh texture |
| $SiO_2$ | 40.46 | 42.85 | 41.80 | 41.53 | 42.97 | 43.10 | 42.43 | 43.40 | 44.99 | 44.90 | 44.14 |
| $TiO_2$ | 0.03 | 0.02 | 0.02 | 0.06 | 0.04 | n.d. | n.d. | 0.04 | 0.03 | 0.02 | n.d. |
| $Al_2O_3$ | 1.55 | 1.04 | 1.45 | 1.87 | 1.80 | 2.32 | 2.14 | 2.38 | 1.46 | 0.74 | 1.19 |
| FeO | 6.65 | 3.61 | 3.59 | 6.71 | 4.71 | 4.07 | 4.75 | 4.07 | 3.21 | 4.14 | 3.87 |
| MnO | 0.08 | 0.07 | 1.27 | 0.11 | 0.08 | 0.14 | 0.18 | 0.09 | 0.09 | 0.01 | 0.06 |
| MgO | 38.41 | 39.80 | 35.15 | 37.68 | 36.72 | 34.99 | 33.57 | 36.14 | 33.42 | 39.80 | 36.23 |
| CaO | 0.02 | 0.04 | 0.11 | 0.05 | 0.05 | 0.04 | n.d. | 0.04 | 0.06 | 0.03 | 0.07 |
| $Na_2O$ | 0.02 | 0.01 | n.d. | 0.01 | n.d. | n.d. | 0.01 | n.d. | 0.01 | 0.01 | 0.01 |
| $K_2O$ | 0.01 | n.d. | n.d. | n.d. | n.d. | 0.01 | n.d. | n.d. | 0.02 | n.d. | 0.01 |
| $Cr_2O_3$ | 2.41 | 0.65 | 0.90 | 0.96 | 0.98 | 2.08 | 2.51 | 1.84 | 1.37 | 0.13 | 0.51 |
| NiO | 0.03 | 0.06 | 0.27 | 0.09 | 0.15 | 0.22 | 0.08 | 0.23 | 0.44 | 0.08 | 0.66 |
| Sum | 89.67 | 88.14 | 84.55 | 89.07 | 87.49 | 86.98 | 85.68 | 88.24 | 85.09 | 89.87 | 86.75 |
| | | | | | | | | | | | |
| Si | 1.895 | 1.989 | 2.033 | 1.944 | 2.016 | 2.030 | 2.037 | 2.015 | 2.142 | 2.039 | 2.079 |
| Ti | 0.001 | 0.001 | 0.001 | 0.002 | 0.001 | 0.000 | 0.000 | 0.001 | 0.001 | 0.001 | 0.000 |
| Al | 0.085 | 0.057 | 0.083 | 0.103 | 0.100 | 0.129 | 0.121 | 0.130 | 0.082 | 0.040 | 0.066 |
| $Fe^{2+}$ | 0.260 | 0.140 | 0.146 | 0.263 | 0.185 | 0.160 | 0.191 | 0.158 | 0.128 | 0.157 | 0.152 |
| Mn | 0.003 | 0.003 | 0.052 | 0.004 | 0.003 | 0.006 | 0.008 | 0.004 | 0.004 | 0.000 | 0.002 |
| Mg | 2.680 | 2.753 | 2.548 | 2.628 | 2.568 | 2.457 | 2.402 | 2.501 | 2.371 | 2.693 | 2.543 |
| Ca | 0.001 | 0.002 | 0.006 | 0.003 | 0.002 | 0.002 | 0.000 | 0.002 | 0.003 | 0.001 | 0.003 |
| Na | 0.001 | 0.001 | 0.000 | 0.001 | 0.000 | 0.000 | 0.001 | 0.000 | 0.001 | 0.001 | 0.001 |
| K | 0.000 | 0.000 | 0.000 | 0.000 | 0.000 | 0.001 | 0.000 | 0.000 | 0.001 | 0.000 | 0.001 |
| Cr | 0.089 | 0.024 | 0.034 | 0.035 | 0.036 | 0.077 | 0.095 | 0.068 | 0.051 | 0.005 | 0.019 |
| Ni | 0.001 | 0.002 | 0.011 | 0.003 | 0.006 | 0.008 | 0.003 | 0.008 | 0.017 | 0.003 | 0.025 |
| Sum | 5.018 | 4.972 | 4.913 | 4.987 | 4.917 | 4.871 | 4.857 | 4.888 | 4.800 | 4.941 | 4.892 |

n.d. not-detected

Table 4. Continued...

| Sample | S2-C3_21 | S2-C3_22 | S2-C3_23 | S2-C3_24 | S2-C3_25 | S2-C4_29 | S2-C4_30 | S2-C4_31 | S2-C5_32 | S2-C5_33 | S2-C5_34 | S2-C5_35 | S2-C7_38 | S2-C7_39 | S2-C7_40 |
|---|---|---|---|---|---|---|---|---|---|---|---|---|---|---|---|
| | vein | vein | vein | mesh texture | mesh texture | bastite | mesh texture | vein | vein | vein | rim mesh texture | core mesh texture | bastite | bastite | core mesh texture |
| $SiO_2$ | 45.85 | 45.49 | 46.47 | 45.23 | 45.41 | 40.04 | 44.23 | 43.82 | 44.33 | 44.43 | 44.44 | 44.09 | 43.06 | 41.18 | 43.84 |
| $TiO_2$ | n.d. | n.d. | 0.01 | n.d. | 0.02 | 0.04 | 0.01 | 0.01 | n.d. | 0.01 | 0.01 | 0.04 | n.d. | 0.04 | 0.01 |
| $Al_2O_3$ | 0.76 | 0.74 | 0.81 | 0.22 | 0.47 | 3.02 | 1.20 | 1.77 | 0.61 | 0.61 | 0.34 | 0.50 | 2.13 | 1.13 | 1.21 |
| FeO | 2.92 | 2.86 | 2.92 | 3.21 | 3.63 | 7.74 | 3.56 | 3.53 | 3.05 | 3.07 | 3.89 | 4.90 | 4.40 | 5.81 | 4.03 |
| MnO | 0.11 | 0.11 | 0.07 | 0.04 | 0.07 | 0.10 | 0.08 | 0.14 | 0.12 | 0.60 | 0.04 | 0.07 | 0.14 | 0.08 | 0.08 |
| MgO | 37.47 | 37.90 | 38.84 | 40.50 | 39.40 | 37.08 | 37.44 | 36.68 | 36.89 | 38.10 | 40.26 | 39.59 | 36.53 | 38.14 | 37.01 |
| CaO | 0.05 | 0.06 | 0.03 | 0.04 | 0.05 | 0.06 | 0.07 | 0.08 | 0.06 | 0.06 | 0.03 | 0.03 | 0.08 | 0.05 | 0.10 |
| $Na_2O$ | n.d. | n.d. | n.d. | 0.01 | n.d. | 0.01 | n.d. | n.d. | 0.01 | 0.02 | 0.01 | 0.01 | 0.01 | 0.02 | 0.01 |
| $K_2O$ | n.d. | n.d. | 0.01 | 0.01 | n.d. | n.d. | 0.01 | 0.01 | n.d. | 0.02 | n.d. | 0.01 | n.d. | n.d. | 0.01 |
| $Cr_2O_3$ | 0.02 | 0.04 | 0.07 | n.d. | 0.06 | 0.98 | 0.53 | 1.37 | 0.01 | n.d. | n.d. | 0.04 | 1.68 | 1.97 | 0.48 |
| NiO | 0.13 | 0.15 | 0.15 | 0.26 | 0.24 | 0.09 | 0.24 | 0.11 | 0.30 | 0.26 | 0.31 | 0.39 | 0.14 | 0.17 | 0.39 |
| Sum | 87.32 | 87.36 | 89.38 | 89.52 | 89.36 | 89.16 | 87.38 | 87.52 | 85.38 | 87.18 | 89.33 | 89.68 | 88.18 | 88.60 | 87.16 |
| | | | | | | | | | | | | | | | |
| Si | 2.118 | 2.103 | 2.099 | 2.055 | 2.068 | 1.887 | 2.061 | 2.041 | 2.103 | 2.073 | 2.034 | 2.023 | 2.006 | 1.939 | 2.056 |
| Ti | 0.000 | 0.000 | 0.000 | 0.000 | 0.001 | 0.001 | 0.000 | 0.000 | 0.000 | 0.000 | 0.000 | 0.001 | 0.000 | 0.002 | 0.000 |
| Al | 0.042 | 0.040 | 0.043 | 0.012 | 0.025 | 0.168 | 0.066 | 0.097 | 0.034 | 0.034 | 0.018 | 0.027 | 0.117 | 0.063 | 0.067 |
| $Fe^{2+}$ | 0.113 | 0.111 | 0.110 | 0.122 | 0.138 | 0.305 | 0.139 | 0.138 | 0.121 | 0.120 | 0.149 | 0.188 | 0.171 | 0.229 | 0.158 |
| Mn | 0.004 | 0.004 | 0.003 | 0.002 | 0.003 | 0.004 | 0.003 | 0.005 | 0.005 | 0.024 | 0.002 | 0.003 | 0.005 | 0.003 | 0.003 |
| Mg | 2.579 | 2.611 | 2.615 | 2.742 | 2.674 | 2.604 | 2.599 | 2.546 | 2.608 | 2.650 | 2.746 | 2.707 | 2.536 | 2.676 | 2.587 |
| Ca | 0.002 | 0.003 | 0.001 | 0.002 | 0.002 | 0.003 | 0.004 | 0.004 | 0.003 | 0.003 | 0.001 | 0.002 | 0.004 | 0.003 | 0.005 |
| Na | 0.000 | 0.000 | 0.000 | 0.001 | 0.000 | 0.001 | 0.000 | 0.000 | 0.001 | 0.002 | 0.001 | 0.001 | 0.001 | 0.002 | 0.001 |
| K | 0.000 | 0.000 | 0.001 | 0.000 | 0.000 | 0.000 | 0.001 | 0.001 | 0.000 | 0.001 | 0.000 | 0.001 | 0.000 | 0.000 | 0.001 |
| Cr | 0.001 | 0.002 | 0.002 | 0.000 | 0.002 | 0.036 | 0.020 | 0.051 | 0.000 | 0.000 | 0.000 | 0.002 | 0.062 | 0.073 | 0.018 |
| Ni | 0.005 | 0.006 | 0.006 | 0.009 | 0.009 | 0.004 | 0.009 | 0.004 | 0.011 | 0.010 | 0.011 | 0.014 | 0.005 | 0.007 | 0.015 |
| Sum | 4.864 | 4.879 | 4.881 | 4.945 | 4.923 | 5.012 | 4.901 | 4.887 | 4.886 | 4.916 | 4.963 | 4.969 | 4.908 | 4.996 | 4.910 |

n.d. not-detected

Table 4. Continued...

| Sample | S2-C7_41 | SP2-C6_184 | SP2-C6_185 | SP2-C6_186 | SP2-C6_187 | SP2-C6_188 | SP2-C6_189 | SP2-C6_190 | SP2-C6_191 | SP2-C6_192 | SP2-C6_193 | SP2-C8_194 | SP2-C8_200 |
|---|---|---|---|---|---|---|---|---|---|---|---|---|---|
| | rim of mesh texture | vein | vein | vein | vein | vein | vein | bastite | bastite | bastite | bastite | bastite | bastite |
| $SiO_2$ | 43.36 | 42.31 | 41.59 | 42.33 | 42.24 | 41.81 | 42.52 | 41.09 | 41.39 | 41.02 | 40.69 | 42.04 | 41.44 |
| $TiO_2$ | 0.02 | n.d. | 0.04 | n.d. | 0.04 | n.d. | 0.03 | 0.12 | 0.11 | 0.12 | 0.11 | 0.06 | 0.32 |
| $Al_2O_3$ | 1.26 | 3.80 | 4.28 | 3.91 | 3.95 | 4.37 | 3.95 | 3.70 | 4.07 | 4.02 | 3.46 | 3.51 | 2.73 |
| FeO | 4.94 | 7.01 | 7.30 | 7.35 | 7.21 | 7.36 | 7.30 | 7.51 | 7.14 | 7.04 | 7.90 | 7.87 | 6.28 |
| MnO | 0.10 | 0.11 | 0.11 | 0.12 | 0.09 | 0.12 | 0.12 | 0.08 | 0.09 | 0.10 | 0.10 | 0.13 | 0.03 |
| MgO | 37.91 | 34.94 | 35.30 | 34.74 | 34.63 | 34.77 | 35.07 | 34.00 | 33.33 | 33.72 | 34.12 | 32.78 | 36.10 |
| CaO | 0.08 | 0.05 | 0.02 | 0.03 | 0.06 | 0.02 | 0.02 | 0.09 | 0.12 | 0.10 | 0.11 | 0.11 | 0.06 |
| $Na_2O$ | 0.03 | n.d. | 0.01 | n.d. | 0.01 | 0.01 | n.d. | 0.01 | 0.01 | 0.02 | 0.01 | 0.02 | 0.04 |
| $K_2O$ | 0.02 | 0.01 | 0.01 | n.d. | 0.01 | n.d. | n.d. | 0.01 | n.d. | 0.01 | n.d. | 0.01 | n.d. |
| $Cr_2O_3$ | 0.34 | 0.03 | 0.02 | 0.03 | 0.02 | 0.01 | 0.04 | 0.47 | 0.44 | 0.50 | 0.51 | 0.33 | 0.67 |
| NiO | 0.29 | 0.14 | 0.16 | 0.20 | 0.16 | 0.16 | 0.15 | 0.46 | 0.46 | 0.45 | 0.37 | 0.50 | 0.22 |
| Sum | 88.33 | 88.41 | 88.83 | 88.71 | 88.43 | 88.63 | 89.21 | 87.54 | 87.16 | 87.09 | 87.37 | 87.37 | 87.89 |
| | | | | | | | | | | | | | |
| Si | 2.019 | 1.981 | 1.944 | 1.979 | 1.979 | 1.957 | 1.975 | 1.960 | 1.975 | 1.961 | 1.950 | 2.006 | 1.957 |
| Ti | 0.001 | 0.000 | 0.001 | 0.000 | 0.002 | 0.000 | 0.001 | 0.004 | 0.004 | 0.004 | 0.004 | 0.002 | 0.011 |
| Al | 0.069 | 0.210 | 0.236 | 0.215 | 0.218 | 0.241 | 0.216 | 0.208 | 0.229 | 0.227 | 0.195 | 0.198 | 0.152 |
| $Fe^{2+}$ | 0.192 | 0.274 | 0.285 | 0.287 | 0.282 | 0.288 | 0.284 | 0.300 | 0.285 | 0.281 | 0.317 | 0.314 | 0.248 |
| Mn | 0.004 | 0.004 | 0.004 | 0.005 | 0.004 | 0.005 | 0.005 | 0.003 | 0.004 | 0.004 | 0.004 | 0.005 | 0.001 |
| Mg | 2.631 | 2.438 | 2.460 | 2.420 | 2.418 | 2.426 | 2.428 | 2.417 | 2.370 | 2.402 | 2.437 | 2.332 | 2.540 |
| Ca | 0.004 | 0.003 | 0.001 | 0.001 | 0.003 | 0.001 | 0.001 | 0.005 | 0.006 | 0.005 | 0.006 | 0.005 | 0.003 |
| Na | 0.002 | 0.000 | 0.001 | 0.000 | 0.001 | 0.001 | 0.000 | 0.001 | 0.001 | 0.002 | 0.001 | 0.001 | 0.004 |
| K | 0.001 | 0.001 | 0.000 | 0.000 | 0.001 | 0.000 | 0.000 | 0.001 | 0.000 | 0.001 | 0.000 | 0.001 | 0.000 |
| Cr | 0.012 | 0.001 | 0.001 | 0.001 | 0.001 | 0.000 | 0.001 | 0.018 | 0.016 | 0.019 | 0.019 | 0.013 | 0.025 |
| Ni | 0.011 | 0.005 | 0.006 | 0.008 | 0.006 | 0.006 | 0.006 | 0.017 | 0.017 | 0.017 | 0.014 | 0.019 | 0.008 |
| Sum | 4.946 | 4.917 | 4.939 | 4.917 | 4.914 | 4.925 | 4.918 | 4.933 | 4.908 | 4.922 | 4.947 | 4.897 | 4.950 |

n.d. not-detected

Table 5. Representative analysis of chlorite.

| Sample | S2-C4_28 | S2-C8_44 | SP2-C3_194 | SP2-C3_195 | SP2-C3_196 | SP2-C3_197 | SP2-C3_198 |
|---|---|---|---|---|---|---|---|
| | spinel rim | spinel rim | spinel rim | spinel rim | spinel rim | spinel rim | spinel rim |
| $SiO_2$ | 38.29 | 41.17 | 19.95 | 20.07 | 23.26 | 30.09 | 26.63 |
| $TiO_2$ | 0.03 | 0.01 | 0.06 | 0.07 | n.d. | 0.02 | 0.06 |
| $Al_2O_3$ | 5.09 | 2.52 | 17.58 | 16.55 | 28.16 | 23.09 | 14.80 |
| $Cr_2O_3$ | 7.37 | 3.11 | 13.68 | 14.69 | 0.56 | 0.06 | 9.09 |
| FeO TOT | 3.76 | 3.77 | 15.44 | 15.92 | 15.70 | 3.76 | 15.52 |
| MnO | 0.11 | 0.11 | 1.05 | 1.06 | 0.32 | 0.05 | 0.43 |
| MgO | 34.36 | 37.97 | 21.47 | 21.12 | 20.41 | 30.63 | 21.20 |
| CaO | 0.04 | 0.05 | 0.15 | 0.06 | 0.02 | 0.01 | 0.02 |
| $Na_2O$ | 0.02 | n.d. | 0.09 | 0.04 | 0.02 | 0.01 | n.d. |
| $K_2O$ | 0.01 | 0.01 | 0.02 | n.d. | 0.01 | n.d. | n.d. |
| Sum | 89.07 | 88.72 | 89.48 | 89.58 | 88.46 | 87.72 | 87.75 |
| | | | | | | | |
| Si | 7.201 | 7.664 | 4.189 | 4.234 | 4.624 | 5.618 | 5.513 |
| Ti | 0.004 | 0.002 | 0.009 | 0.012 | 0.000 | 0.002 | 0.009 |
| Al | 1.128 | 0.553 | 4.350 | 4.115 | 6.598 | 5.080 | 3.611 |
| Cr | 1.644 | 0.687 | 3.406 | 3.675 | 0.131 | 0.012 | 2.231 |
| Fe | 0.591 | 0.587 | 2.711 | 2.808 | 2.610 | 0.587 | 2.686 |
| Mn | 0.017 | 0.017 | 0.186 | 0.189 | 0.054 | 0.008 | 0.076 |
| Mg | 9.634 | 10.537 | 6.721 | 6.643 | 6.049 | 8.526 | 6.542 |
| Ca | 0.008 | 0.009 | 0.034 | 0.013 | 0.005 | 0.003 | 0.004 |
| Na | 0.007 | 0.000 | 0.035 | 0.015 | 0.009 | 0.005 | 0.001 |
| K | 0.003 | 0.002 | 0.005 | 0.000 | 0.002 | 0.000 | 0.000 |
| Sum | 20.236 | 20,059 | 21.647 | 21.705 | 20.082 | 19.842 | 20.674 |
| | Tlc-Chl* | Tlc-Chl* | Crp* | Crp* | Crp* | Cch* | Shr* |

n.d. not-detected

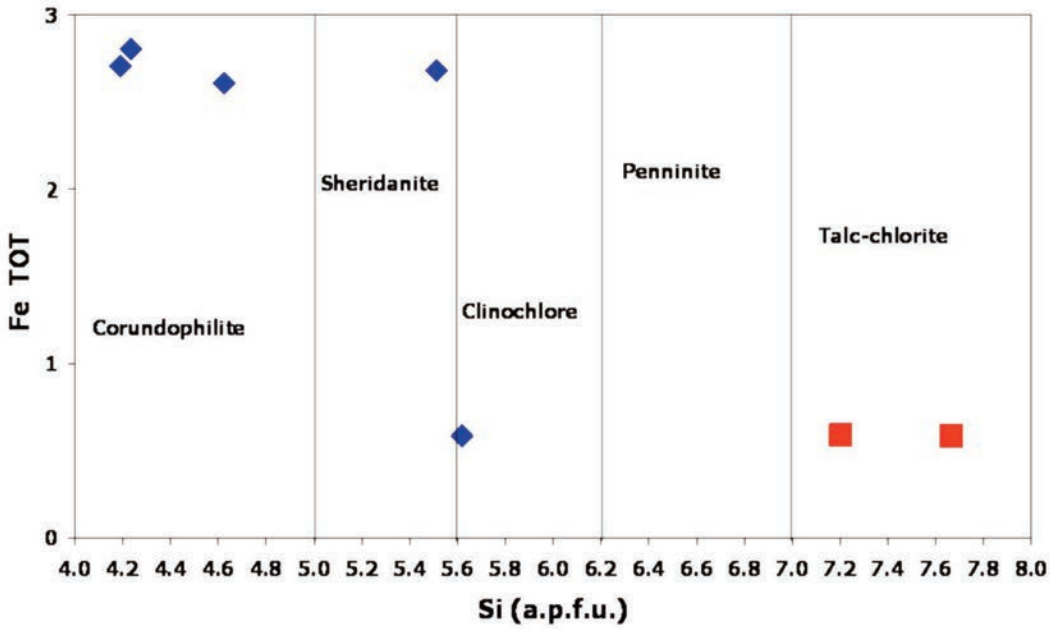


Figure 14. Chemical composition of chlorite in the FU serpentinite; chlorite nomenclature after Hey (1954). Symbols: square for S2 (massive serpentinite); diamond for SPR2 (cataclastic serpentinite).

interpreted as responsible for a volume increase, that in turn accounts for the density decreasing in serpentinite when comparing with the original peridotite; nevertheless, the problem of volume increase due to hydration is still debated (O'Hanley, 1992). The third serpentinization event of the studied serpentinites could be related to the orogenic evolution and is attested by the occurrence of transtensional veins with the opening of micro-pull-aparts filled with serpentine fibers although an oceanic origin for such tectonic structure cannot be ruled out.

Relict clinopyroxene is commonly rimmed by amphibole (probably of the tremolite-actinolite series). Occurrence of tremolite + talc at the expense of pyroxenes has been observed in peridotite samples from the Mid Atlantic Ridge (Bach et al., 2004). Although talc has never been detected in our samples, our finding suggests that crystallization of tremolite-actinolite in the Frido Unit serpentinites may have occurred during oceanic alteration. In order to estimate the conditions of serpentinization, several indicators are commonly used, such as the mineralogy of serpentine species, but the precision is poor because the stability field of serpentine types is not well constrained (Bach et al., 2004 and references therein).

Here we suggest to consider the chemical composition of spinel, in order to unravel the metamorphic evolution of the FU serpentinites.

The analyzed spinel shows a holly-leaf habit, interpreted as being characteristic of the mantle porphyroclastic tectonites (Nicolas and Mercier, 1975). Spinel has been commonly used as a petrogenetic indicator of mantle melting degree, provided it has not reacted with percolating melts or differently altered (Tartarotti et al., 2002 and

references therein). The analyzed spinel crystals from the FU serpentinites are chemically zoned, being characterized by relatively lower Cr content at the crystal core (Cr# ranging between 43 and 46), and higher Cr content at the rim (Cr# ranging between 87 and 93; see Table 2).

Values of Cr# < 60 have been found in abyssal peridotites and in Type I alpine-peridotites (e.g., Dick and Bullen, 1984; Haggerty, 1991), and related to the lithospheric mantle emplaced near the ocean ridge. According to Dick and Bullen (1984), higher values of Cr# (i.e., Cr# > 60) can be found in modern arc-related volcanic settings and in certain alpine-type ophiolites (Type III-ophiolites) that are consequently interpreted as related to a sub-volcanic arc petrogenesis.

The FU spinel crystals are chemically zoned not only in terms of Cr, but also of Al, and Fe; the rim is a ferritchromite. NiO, although occurring in small percentages, is higher in the chromite portions than in ferritchromite. According to Barnes (2000), chromites that have been affected by amphibolite facies metamorphism are enriched in Zn and Fe, whilst chromites that have been affected by low temperature metamorphism are poorer in Ni contents. According to the same Authors, trivalent ions $Cr^{3+}$, $Al^{3+}$, $Fe^{3+}$ should not be sensible to the amphibolite facies metamorphism, although $Fe^{3+}$ should decrease during the low-temperature alteration characterized by talc-carbonate-enrichment. Other Authors (Barnes and Roeder, 2001) state that Al-poor chromites are of metamorphic origin and call "ferritchromite" the metamorphic, Al-poor chromite. Infact, during seafloor alteration, magnetite and chromite would react with silicates and fluids giving rise to chlorite and amphibole.

Swanson (2004) suggests that Cr-Fe-oxides in ultramafic rocks record the physical conditions of metamorphic evolution. According to the same Author, concurrent enstatite and tremolite in ultramafic rocks would be consistent with amphibolite facies metamorphic conditions (Swanson, 2004). Retrogression from the amphibolite to greenschists facies metamorphic conditions should be recorded in ultramafic rocks by progressive hydration and recrystallization of Cr-Fe-oxides (Swanson, 2004).

Mellini et al. (2005) suggest that ferritchromite is of hydrothermal origin formed after the oceanic serpentinization within the chlorite stability field. Al-rich spinel would be replaced by ferritchromite through dissolution-crystallization processes. Such ferritchromite is not a single phase, but it is rather a complex association of Cr-magnetite + chlorite/lizardite, as deduced by TEM analysis (Mellini et al., 2005). The occurrence of chlorite and/or lizardite intergrowth with ferritchromite could easily explain the anomalous high $SiO_2$ contents in ferritchromite analyzed in the present paper (see Table 2), although this inference should be supported by additional investigations, such as TEM analyses. Mellini et al. (2005) have also described chlorite rimming the ferritchromite crystals which they interpret as due to metasomatic reactions of serpentine in the mesh texture with a steptochlorite composition devoloped at temperatures definitely higher than 350-450 °C.

Other Authors, such as Merlini et al. (2009) state that metamorphism can change the chromite composition provided that temperature is as high as 300 °C; under such conditions, chromite generates Cr-rich chlorite and ferritchromite. According to Merlini et al. (2009) the occurrence of mineral phases as serpentine, ferritchromite and Cr-chlorite can be explained by hydration and oxidation reactions consuming Al-rich chromite during prograde metamorphism. Finally, ferritchromite as alteration product of Cr-spinel has also been observed in oceanic peridotites from the Atlantic ocean (Bach et al., 2004).

By considering the interpretations given by several Authors, we infer that the Al-rich spinel core could be representative of the original

lithospheric mantle spinel-peridotite; the Al-poor rim with a ferritcromite composition could have been produced, together with Cr-chlorite, by metamorphic reactions occurred during hydrothermal alteration in the Tethyan oceanic realm at the expense of original mantle Al-rich spinel.

The oceanic evolution of the FU serpentinites has been followed by the orogenic history related to the building of the Apennine chain. This latest step is attested by the occurrence of veins filled with prehnite cutting through all the previous textures, in accord with prevous studies (e.g., Sansone and Rizzo, 2012). If compared with other rocks of the FU, and, in particular, with metadolite dykes still preserving relict oceanic minerals (Sansone, 2009; Sansone et al., 2010), the studied serpentinites show, at least in part, a common oceanic evolution, characterized by greenscist facies minerals (e.g., amphibole of the tremolite-actinolite series). By contrast, the blueschist orogenic minerals (e.g., lawsonite and Na-rich amphibole; Sansone et al., 2011; Sansone et al., 2012 in prep.) detected in the metadolerite dykes have not been observed in the FU serpentinites. Finally, the latest orgenic steps developing veins filled with minerals of the prehnite-pumpellyite facies are characteristic features of both serpentinites and metadolerite dykes.

## Concluding remarks

Serpentinites of the Frido Unit (Southern Apennines) derive from serpentinization of mantle peridotites (lherzolite and subordinately harzburgite) equilibrated under the spinel-peridotite facies and characterized by a porphyroclastic texture. This interpretation is inferred from the observations of textural and mineralogical features, namely: i) relict primary mineralogy, as spinel with holly-leaf habit, olivine, orthopyroxene (fresh crystal and exolutions within clinopyroxene), and clinopyroxene porphyroclasts; ii) porphyroclastic olivine and orthopyroxene easily identifiable for being replaced by serpentine pseudomorphs; iii) chemical composition of the spinel core; iv) extensive serpentinization occurred mainly under static condition developing a typical mesh texture, and extensional veins. Amphibole rimming clinopyroxene or replacing orthopyroxene is inferred to be related to oceanic alteration under probably greenschist facies conditions. The composition of spinel reveals that this oxide has reacted with hydrothermal fluids under temperature conditions probably higher than 300 °C (i.e., consistent with greenschist facies conditions) producing ferritchromite at the crystal rims and Cr-chlorite coronae. All these evidence concur to interpret the Frido Unit serpentinites as deriving from a lithospheric mantle that has extensively reacted with (seawater-derived) hydrothermal fluids. Further investigations would be needed for determining the nature and compositions of the fluids and for evaluating the physical conditions of the oceanic alteration.

The orogenic metamorphic history of the FU serpentinites is recorded by LT metamorphic minerals, such as prehnite filling late-stage veins, as observed in the surrounding rocks of the same tectonic unit.

## Acknowledgments

The authors thanks L. Gaggero and an anonymous reviewer for their helpful comments. The paper has benefited from the comments of Editor G.B. Andreozzi to whom we are grateful. University of Basilicata research funds are acknowledged.

## References

Amodio-Morelli L., Bonardi G., Colonna V., Dietrich D., Giunta G., Ippolito F., Liguori V., Lorenzoni S., Paglianico A., Perrone V., Piccarreta G., Russo M., Scandone P., Zanettin-Lorenzoni E. and Zuppetta A. (1976) - L'arco Calabro-Peloritano nell'orogene Appenninico-Maghrebide. *Memorie della Società Geologica Italiana*, 17, 1-60.

Aumento F. and Loubat H. (1971) - The Mid-Atlantic Ridge near 45 °N: serpentinized ultramafic intrusions. *Canadian Journal Earth Sciences*, 8, 631-663.

Bach W., Garrido C.J., Paulick H., Harvey J. and Rosner R. (2004) - Seawater-peridotite interactions: First insights fron OPD Leg 209, MAR 15°N. *Geochemistry, Geophysics, Geosystems*, 5, 1-22, Q09F26, doi: 10.1029/ 2004GC000744.

Barnes S.J. (2000) - Chromite in Komatiites, II: Modification during greenschist to mid-anfibolite facies metamorphism. *Journal of Petrology*, 41, 387-409.

Barnes S.J. and Roeder P.L. (2001) - The range of spinel compositions in terrestrial mafic and ultramafic rocks. *Journal of Petrology*, 42, 2279-2302.

Boillot G., Féraud G., Recq M. and Girardeau J. (1989) - Undercrusting by serpentinites beneath rifted margins. *Nature*, 341, 523-525.

Boillot G., Girardeau J. and Kornoprobst J. (1988) - Rifting of the Galicia margin: crustal thinning and emplacement of mantle rocks on the seafloor. In: Proceedings ODP Sci. Results, Ocean Drilling Program. (eds): G. Boillot and E.L. Winter, 103, 741-756.

Bonardi G., Amore F.O., Ciampo G., De Capoa P., Miconnét P. and Perrone V. (1988) - Il Complesso Liguride Auct.: Stato delle conoscenze attuali e problemi aperti sulla sua evoluzione Pre-Appenninica ed i suoi rapporti con l'Arco Calabro. *Memorie della Società Geologica Italiana*, 41, 17-35.

Bonardi G., Ciarcia S., Di Nocera S., Matano F., Sgrosso I. and Torre M. (2009) - Carta delle principali unità cinematiche dell'Appennino meridionale. Nota illustrativa. *Italian Journal of Geosciences*, 128, 47-60.

Bonatti E. (1968) - Ultramafic rocks from the Mid-Atlantic Ridge. *Nature*, 219, 363-264.

Bonatti E. (1976) - Serpentinite protrusion from Mid-Atlantic Ridge. *Earth and Planetary Science Letters*, 32, 107-113.

Cannat M. (1996) - How thick is the magmatic crust at slow spreading oceanic crust? *Journal of Geophysical Research*, 101, 2847-2857.

Cannat M., Lagabrielle Y., Bougault H., Casey J., de Coutures N., Dmitriev L. and Fouquet Y. (1997) - Ultramafic and gabbroic exposures at the Mid-Atlantic Ridge: geological mapping in the 15°N region. *Tectonophysics*, 279, 193-213.

Cavalcante F., Belviso C., Finizio F., Lettino A. and Fiore S. (2009) - Carta geologica delle Unità Liguridi dell'area del Pollino (Basilicata): nuovi dati geologici, mineralogici e petrografici. © REGIONE BASILICATA-Dipartimento Ambiente, Territorio e Politiche della Sostenibilità. Ed. S. FIORE. ISBN: 978-88-7522-026-6.

Cello G. and Mazzoli S. (1999) - Appenine tectonics in southern Italy: A review. *Journal of Geodynamics*, 27, 191-211.

Cortesogno L., Gaggero L. and Molli G. (1994) - Ocean floor tectono-metamorphic evolution in the Piedmont-Liguride Jurassic basin: a review. *Memorie della Società Geologica Italiana*, 48, 151-163.

Dick H.J.B. and Bullen T. (1984) - Chromian spinel as a petrogenetic indicator in abyssal and alpine-type peridotites and spatially associated lavas. *Contributions to Mineralogy and Petrology*, 86, 54-76.

Di Leo P., Schiattarella M., Cuadros J. and Cullers R. (2005) - Clay mineralogy, geochemistry and structural setting of the ophiolite-bearing units from Southern Italy: a multidisciplinary approach to asses tectonics history and exhumation modalities. *Atti Ticinensi di Scienze della Terra S.S.*, 10, 87-93.

Doglioni C., Gueguen E., Harabaglia P. and Mongelli F. (1999) - On the origin of west-directed subduction zones and applications to the western Mediterranean. In: The Mediterranean basins: Tertiary extension within the alpine orogen. (eds): B. Durand, L. Jolivet F., Horváth and M. Séranne, *Special Publications Geological Society*, London, 156, 541-561.

Driesner T. (1993) - Aspects petrographical, structural and stable isotope geochemical evolution of ophicarbonate breccias from ocean floor to subduction and uplift: an example from Chatillion, Middle Aosta Valley, Italian Alps. *Schweizer Mineralogische und Petrographische Mitteilungen*, 73, 69-84.

Escartin J., Hirth G. and Evans B. (1997) - Effects of serpentinization on the lithosphere strength and the style of normal faulting at slow spreading ridges, *Earth and Planetary Science Letters*, 151, 181-190.

Gueguen E., Doglioni C. and Fernandez M. (1998) - On the post-25 Ma geodynamic evolution of the western

Mediterranean. *Tectonophysics*, 298, 259-269.

Haggerty S.E. (1991) - Oxide mineralogy of the upper mantle. *Review in Mineralogy and Geochemistry*, 25, 335-416.

Hey M.H. (1954) - A new review of the chlorites. *Mineralogical Magazine*, 30, 224-292.

Invernizzi C., Bigazzi G., Corrado S., Di Leo P., Schiattarella M. and Zattin M. (2008) - New thermobaric constraints of the exhumation history of the Liguride accretionary wedge, Southern Italy. *Ofioliti*, 33, 21-32.

Juteau T., Berger E. and Cannat M. (1990):- Serpentinized, residual mantle peridotites from the M.A.R. Median Valley, ODP Hole 670A (21°10'N, 45°02'W, Leg 109): primary mineralogy and geothermometry. In: R.S. Detrick; J. Honnorez, W.B. Bryan, T. Juteau et al. (eds.), Proceedings of the Ocean Drilling Program, Scientific Results, College Station, TX (Ocean Drilling Program), 106/109, 27-45, doi:10.2973/odp.proc.sr.106109.117.1990.

Karson J.A., Thompson G., Humphris S.E., Edmonds J.M., Bryan W.B., Brown J.R., Winters A.T., Pockalny R.A., Casey J.F., Campbell A.C., Klinkhammer G., Palmer M.R., Kinzler R.J. and Sulanowska M.M. (1987) - Along axis variation in seafloor spreading in the MARK area. *Nature*, 328, 681-685.

Kelemen P.B., Kikawa E., Miller D.J. (2004) - Proc. ODP, Init. Repts., 209: College Station, TX (Ocean Drilling Program), doi:10.2973/odp.proc.ir.209.2004.

Knott S.D. (1987) - The Liguride Complex of Southern Italy-a Cretaceus to Paleogene accretionary wedge. *Tectonophysics*, 142, 217-226.

Knott S.D. (1994) - Structure, kinematics and metamorphism in the Liguride Complex, Southern Apennine, Italy. *Journal of Structural Geology*, 16, 1107-1120.

Lagabrielle Y., Polino R., Auzende J.M., Blanchet R., Caby R., Fudral S., Lemoine M., Mével C., Ohnenstetter M., Robert D. and Tricart P. (1984) - Les témoins d'une tectonique intraocéanique dans les domaine Tethysien: analyse des rapports entre les ophiolites et leur couvertures metasédimentaires dans la zone des Alpes franco-italiennes. *Ofioliti*, 9, 67-88.

Lagabrielle Y. and Cannat M. (1990) - Alpine Jurassic ophiolites resemble the modern central Atlantic basement. *Geology*, 18, 39-322.

Lagabrielle Y. and Lemoine M. (1997) - Alpine, Corsican, Apennine ophiolites: the slow-spreading ridge model. Ophiolites des Alpes, de Corse et des dorsales lentes. *Comptes Rendus de l'Académie des Sciences.* Paris, 325, 909-920.

Lanzafame G., Spadea P. and Tortorici L. (1979) - Mesozoic ophiolites of northern Calabria and Lucanian Apennine (Southern Italy). *Ofioliti*, 4, 173-182.

Lanzafame G., Spadea P., Tortorici L. (1978) - Provenienza ed evoluzione dei Flysch Cretacico-Eocenici della regione Calabro-Lucana. II: Relazioni tra ofioliti e Flysch Calabro-Lucano. *Ofioliti*, 3, 189-210.

Laurita S. (2008) - Il prisma di accrezione Liguride affiorante al confine Calabro-Lucano: studio termocronologico e strutturale. Tesi di Dottorato, Università degli Studi della Basilicata, 169 pp.

Laurita S., Cavalcante F., Belviso C., Prosser G. (2009) - The Liguride Complex of the Pollino area (southern Apennines): tectonic setting and preliminary mineralogical data. *Rendiconti online Società Geologica Italiana*, 5, 111-114.

Lemoine M., Tricart P. and Boillot G. (1987) - Ultramafic and gabbroic ocean floor of the Ligurian Tethys (Alps, Corsica, Apennines): in search of genetic model. *Geology*, 15, 622-625.

Magde L.S., Barclay A.H., Toomey D.R., Detrick R.S. and Collins J.A. (2000) - Crustal magma plumbing within a segment of the Mid-Atlantic Ridge, 35°N. *Earth and Planetary Science Letters*, 175, 55-67.

Mellini M., Rumori C. and Viti C. (2005) - Hydrothermally reset magmatic spinels in retrograde serpentinites: formation of "ferritchromit" rims and chlorite aureoles. *Contributions to Mineralogy and Petrology*, 149, 266-275.

Mercier J.C.C. and Nicolas A. (1975) - Textures and fabric of upper-mantle peridotites as illustrated by xenoliths from basalts. *Journal of Petrology*, 16, 454-487.

Merlini A., Grieco G. and Diella V. (2009) - Ferritchromite and chromian-chlorite in mélange-hosted Kalkan chromitite (Southern Urals, Russia). *American Mineralogist*, 94, 1459-1467.

Mével C (2003) - Serpentinization of abyssal peridotites at mid-ocean ridges. C.R. Geoscience, 335, 825-852.

Mével C., Cannat M., Gente P., Marion E., Auzende J.M.and Karson J.A. (1991) - Emplacement of deep rocks on the west median valley wall of the MARK

area. *Tectonophysics*, 190, 31-53.

Miyashiro A., Shido F. and Ewing M. (1969) - Composition and origin of serpentines from the Mid-Atlantic Ridge near 24 and 30°N. *Contributions to Mineralogy and Petrology*, 23, 117-127.

Monaco C. (1993) - Le Unità Liguridi nel confine Calabro-Lucano (Appennino Meridionale): controllo dei dati esistenti, nuovi dati ed interpretazione. Bollettino della Società Geologica Italiana, 112, 751-769.

Monaco C., Tansi C., Tortorici L., De Franceso A.M. and Morten L. (1991) - Analisi geologico-strutturale dell'Unità del Frido al confine calabro-lucano (Appennino Meridionale). *Memorie della Società Geologica Italiana*, 47, 341-353.

Monaco C. and Tortorici L. (1994) - Evoluzione geologico-strutturale dell'Appennino Calabro-Lucano. In: F., Ghisetti, C. Monaco, L. Tortorici and L. Vezzani. Strutture ed evoluzione del settore del Pollino (Appennino Calabro-Lucano). Università degli Studi di Catania, Istituto di Geologia e Geofisica. Guida all'escursione. 9-50.

Monaco C. and Tortorici L. ( 1995) - Tectonic role of ophiolite-bearing terranes in building of the Southern Apennines orogenic belt. *Terra Nova*, 7, 153-160.

Monaco C. Tortorici L., Morten L., Critelli S., Tansi C. (1995). Geologia del versante Nord-orientale del Massiccio del Pollino (Confine calabro lucano). Nota illustrativa sintetica alla scala 1:50.000. Boll. Soc. Geol. It. 114, 277-291.

Morimoto N. (1988) - Nomenclature of pyroxenes. *Mineralogy and Petrology*, 39, 55-76.

Morimoto N. (1989) - Nomenclature of pyroxenes. *Canadian Mineralogist*, 27, 143-156.

O'Hanley D.S. (1992) - Solution to the volume problem in serpentinization. *Geology*, 20, 705-708.

Ogniben L. (1969) - Schema introduttivo alla geologia del confine calabro-lucano. *Memorie della Società Geologica Italiana*, 8, 453-763.

Patacca E. and Scandone P. (2007) - Geology of the southern Apennines. In: Results of the CROP Project, Sub-project CROP-04 Southern Apennines (Italy). (eds): A. Mazzotti, E. Patacca and P. Scandone. *Bollettino della Società Geologica Italiana*, Special Issue, 75-119.

Piedilato S. and Prosser G. (2005). -Thrust sequences and evolution of the external sector of a fold and thrust belt: An example from the Southern Apennines (Italy). *Journal of Geodynamics*, 39, 386-402.

Prichard H.M. (1979) - A petrographic study of the process of serpentinisation in ophiolites and the ocean crust. *Contributions to Mineralogy and Petrology*, 68, 231-241.

Rabain A., Cannat M., Escartín J., Pouliquen G., Deplus C. and Rommevaux-Jestin C. (2001) - Focussed volcanism and growth of slow spreading segment (Mid-Atlantic Ridge, 35°N). Earth and Planetary Science Letters, 185, 211-224.

Sansone M.T.C. (2006) - Studio petrografico e geochimico delle rocce basiche presenti nelle scaglie ofiolitiche del Complesso Liguride al confine calabro-lucano. Degree Thesis, Università degli Studi della Basilicata, 216 pp.

Sansone M.T.C. (2009) - Serpentiniti e metadoleriti dell'Unità del Frido: genesi, evoluzione e problematiche ambientali. Ph.D. Thesis, Università degli Studi della Basilicata, 158 pp.

Sansone M.T.C., Rizzo G. and Mongelli G. (2011) - Mafic rocks from ophiolites of the Liguride units (Southern Apennines): petrographical and geochemical characterization. *International Geology Review,* 53, 130-156, doi: 10.1080/00206810902954993.

Sansone M.T.C., Prosser G., Rizzo G. and Tartatotti P. (2010) - Oceanic evolution of Spl-Peridotites of The Frido Unit Ophiolites (southern Apennine-Italy). Geophysical Reaserch Abstracts, 12, EGU2010-13316-EGU GENERAL ASSEMBLY 2010© AUTHOR(S).

Sansone M.T.C. and Rizzo G. (2012) - Pumpellyite veins in the metadolerite of the Frido Unit (Southern Apennines, Italy). In press into *Periodico di Mineralogia*.

Sansone M.T.C, Tartarotti P., Rizzo G. and Prosser G. (2012) - From ocean to subduction: the polyphase metamorphic evolution of the Frido Unit metadolerite dykes (Southern Apennine, Italy). In: (Eds.) Guido Gosso, Maria Iole Spalla, and Michele Zucali, Multiscale structural analysis devoted to the reconstruction of tectonic trajectories in active margins, Journal of the Virtual Explorer, Electronic Edition, ISSN: 1441-8142, volume 40, paper 4.

Siivola J. and Schmid R. (2007) - List of mineral abbreviations- Recommendations by the IUGS Subcommission on the Systematics of Metamorphic

Rocks: 12. Web version 01.02.07.

Spadea P. (1976) - I carbonati nelle rocce metacalcaree della Formazione del Frido della Lucania. *Ofioliti*, 1, 431-456.

Spadea P. (1982) - Continental crust rock associated with ophiolites in Lucanian Apennine (Southern Italy). *Ofioliti*, 7, 501-522.

Spadea P. (1994) - Calabria-Lucania ophiolites. Bollettino di Geofisica Teorica ed Applicata, 36, 271-281.

Swanson S.E. (2004) - Variation in chromite composition with metamorphic grade, an example from ultramafic rocks from the Spruce Pine district, North Carolina. Geological Society of America, 36, 135. Abstract.

Tartarotti P., Susini S., Nimis P. and Ottolini L. (2002) - Melt migration in the upper mantlealong the Romanche Fracture Zone (Equatorial Atlantic). *Lithos*, 63, 125-149.

Tartarotti P., Benciolini L. and Monopoli B. (1998) - Brecce serpentinitiche nel massiccio ultrabasico del Monte Avic (Falda Ofiolitica Piemontese): possibili evidenze di erosione sottomarina. *Atti Ticinensi di Scienze della Terra S.S.*, 7, 73-86.

Tortorici L., Catalano S. and Monaco C. (2009) - Ophiolite-bearing mélanges in southern Italy. *Geological Journal*, 44, 153-166.

Treves B. and Harper G.D. (1994) - Exposure of serpentinites on the ocean floor: sequences of faulting and hydrofracturing in the Northern Apennine ophiolites. *Ofioliti*, 19, 435-466.

Vezzani L. (1966) - La sezione tortoniana di Perosa sul fiume Sinni presso Episcopia (Potenza). *Geologica Romana*, 5, 263-290.

Vezzani L. (1969) - La Formazione del Frido (Neocomiano-Aptiano) tra il Pollino ed il Sinni. *Geologica Romana*, 8, 129-176.

Vezzani L. (1970) - Le ofioliti della zona tra Castelluccio Inferiore e S. Severino Lucano (Potenza). *Accademia Gioenia di Scienze Naturali in Catania*, 7, 1-49.

Wicks F.J. and Whittaker E.J.W. (1977) - Serpentine texture and serpentinization. *Canadian Mineralogist*, 15, 459-488.

Wicks F.J., Whittaker E.J.W. and Zussman J. (1977) - Idealized model for serpentine textures after olivine. *Canadian Mineralogist*, 15, 446-458.

*Submitted, September 2011 - Accepted, January 2012*